NASA TECHNICAL NOTE

NASA TN D-2584

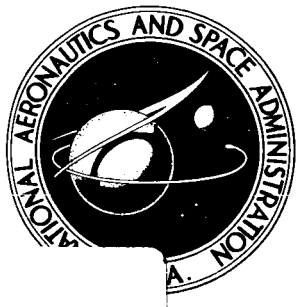

NASA TN D-2584

SOME EFFECTS OF UNCERTAINTIES IN ATMOSPHERE STRUCTURE AND CHEMICAL COMPOSITION ON ENTRY INTO MARS

by Robert L. McKenzie

Ames Research Center

Moffett Field, Calif.

NATIONAL AERONAUTICS AND SPACE ADMINISTRATION • WASHINGTON, D. C. • JANUARY 1965

SOME EFFECTS OF UNCERTAINTIES IN ATMOSPHERE STRUCTURE AND CHEMICAL COMPOSITION ON ENTRY INTO MARS

By Robert L. McKenzie

Ames Research Center
Moffett Field, Calif.

NATIONAL AERONAUTICS AND SPACE ADMINISTRATION

For sale by the Office of Technical Services, Department of Commerce,
Washington, D.C. 20230 -- Price $2.00

SOME EFFECTS OF UNCERTAINTIES IN ATMOSPHERE STRUCTURE AND CHEMICAL COMPOSITION ON ENTRY INTO MARS

By Robert L. McKenzie

Ames Research Center
Moffett Field, Calif.

SUMMARY

The purpose of this study is to provide examples of the degree to which uncertainties in the structure and composition of the martian atmosphere affect various aspects of entry. The discussion contains the effects on manned-vehicle entry corridors, aerodynamic heating, including shock-layer radiation for an unmanned probe-type entry, and vehicle design requirements for an unmanned probe soft landing. The results indicate that current uncertainties in atmosphere scale height are significant in that they greatly decrease the entry corridor heights for manned vehicles. Uncertainties in the atmosphere composition and scale height are shown to preclude accurate prediction of the heating rates for an unmanned probe entry. However, as expected, requirements for soft landings are the most restrictive. Already difficult to satisfy because of low surface pressure, these requirements become extremely limiting because of the uncertainty in atmosphere structure.

INTRODUCTION

Recent studies clearly establish that entry vehicle design and trajectory analysis depend on composition and structure of the planetary atmosphere (refs. 1 and 2). However, there are many widely different current estimates of these quantities for the atmosphere of Mars. The question then arises as to the effects of these uncertainties on an entry analysis. This has been answered in part by Spiegel (ref. 1) who investigated the uncertainty effects on entry vehicle weights and size. Adams et al. (ref. 2) also discussed the uncertainty effects on aerodynamic heating and vehicle design and outlined some of the other problems associated with planetary entry. Peterson and Tobak (ref. 3) analyzed the tumbling and large amplitude oscillations of an entering vehicle and showed the atmosphere structure to have little effect on the oscillatory behavior of the vehicle.

It is the purpose of this report to discuss more generally the martian atmosphere uncertainties and to illustrate the degree to which these uncertainties affect the entry corridors for a manned vehicle, the aerodynamic heating for an unmanned probe entry, and the vehicle design requirements for insuring low velocities near the planet's surface (hereafter referred to as the "landing problem"). These examples help to define the significance of the atmosphere uncertainties. The atmosphere extremes used for this study were chosen as representative and do not include all available estimates to date.

SYMBOLS

A	aerodynamic coefficient reference area, ft^2
C_D	aerodynamic drag coefficient, $\frac{2D}{\rho_\infty A V_\infty^2}$
D	aerodynamic drag, lb
g	local acceleration due to gravity, ft/sec^2
$\bar{g}$	gravitational constant, 32.17 ft/sec^2
G	vehicle deceleration divided by $\bar{g}$
h	enthalpy, Btu/lb
h_p	periapsis altitude, ft
h_p'	new value of h_p resulting from a change in an atmosphere or aerodynamic parameter
H	isothermal scale height, ft
I	total radiant intensity behind bow shock, Btu/ft^3 sec
J	mechanical equivalent of heat, 778 ft-lb/Btu
l	reference length for Reynolds number, ft
L	aerodynamic lift, lb
m	vehicle mass, slugs
$\bar{m}$	mean molecular weight of atmosphere
p	pressure, lb/ft^2 unless otherwise noted
$\dot{q}$	stagnation-point heating rate, Btu/ft^2 sec
r	distance from planet center, ft
R_N	vehicle nose radius, ft
R_∞	Reynolds number based on ambient stream conditions
T	temperature, ^oR
V	vehicle velocity, ft/sec
$\bar{V}$	ratio of vehicle velocity to local circular velocity, $\frac{V}{V_c}$ (where $V_c = \sqrt{gr}$)
δ	shock-layer thickness, ft
γ	atmosphere gas specific heat ratio
φ	flight-path angle measured from local horizontal, deg
ρ	density, $slugs/ft^3$

ρ_{ref} atmosphere reference density, slugs/ft^3

$\rho_{SL_\oplus}$ standard earth sea-level density, 2.377×10^{-3} slugs/ft^3

Δh_p corridor depth: difference in periapsis altitude between the overshoot and undershoot corridor bounds for a given entry speed, millions of feet

Subscripts

c circular; also, convective

exit conditions upon leaving or exiting the atmosphere (measured at the same altitude as entry conditions)

i initial or entry

r radiative

s stagnation point

surf planet surface

strat stratosphere

w wall

∞ ambient stream

ANALYSIS

The problems of entry treated in this report are individual and nearly independent, each dealing with a different aspect of martian entry. The only dependence or similarity lies in the magnitude of the atmosphere uncertainties used for each study. The first section of this analysis defines the atmosphere parameters of interest and the uncertainties contained in them. It is followed by three independent sections discussing the atmosphere uncertainty effects on entry corridors for a manned vehicle, aerodynamic heating during an unmanned probe entry, and the soft landing of an unmanned probe. Each example is chosen to illustrate the effect of the atmosphere uncertainties on one factor in vehicle design without complication due to other aerothermodynamic effects (e.g., lift modulation, heat-shield ablation, etc.).

In keeping with this simplified approach, the entering vehicle was assumed to be a point-mass object approaching a spherical planet. Only planar trajectories into a nonrotating atmosphere were considered. The computing necessary for this analysis was done on a high-speed digital computer which numerically solved the exact differential equations of motion.

Atmosphere Uncertainties

The parameters associated with entry vehicle design or trajectory analysis are usually formulated so that the variables pertaining to atmosphere structure and those defining its composition can be separated.

Structure.- The primary variables related to atmosphere structure which influence the vehicle design or trajectory analysis are density and its variation with altitude. The density variation is conveniently described in terms of the parameters, scale height and reference density, which can be defined with the aid of figure 1, and the equation

$$\rho = \rho_{ref} e^{-\frac{\text{altitude}}{H}}$$

Scale height, H, is represented by the slope of the curve in a plot of the natural logarithm of local density as a function of altitude. For a constant scale height atmosphere, $\log_e \rho$ versus altitude will appear as a straight line with its slope equal to -H. Examples of a constant scale height are illustrated in figure 1 for altitudes above the indicated tropopause of each atmosphere structure. As can be seen, a low scale height results in a "shallow" or more compressed atmosphere than that for a large scale height or "deep" atmosphere. Reference density (ρ_{ref}) can be thought of as the hypothetical surface density that would exist if the atmosphere were of constant scale height all the way to the planet's surface. It is represented in figure 1 by the continuation of the straight-line portion of the density-altitude curve to zero altitude level.

The atmosphere structures plotted in figure 1 represent the extremes chosen for this study. Density is given as a ratio of Mars local density to the standard earth sea-level value. This choice of extreme atmospheres originated from consideration of the estimates and proposed structural models of references 1, 4, 5, and 6, and some unpublished Jet Propulsion Laboratory models (fig. 2). Reference 4 combined estimates of some basic atmosphere parameters to generate extremes based on a surface pressure range of 41 to 132 millibars. Reference 1 contains a series of structural models within these extremes. The unpublished Jet Propulsion Laboratory models followed nearly the same extremes in all variables but used a surface pressure range of 11 to 30 millibars based on the data of reference 6. (The surface pressures in ref. 6 are estimated to be 10 to 40 millibars as a result of recent observations by improved techniques.) The atmosphere structures used in this study are, in effect, the two extreme atmospheres of reference 4 plus the same two atmospheres with densities lower by an order of magnitude (to account for the recent low surface pressure estimates). These four choices bracket an order of magnitude uncertainty in reference density and a factor of 2.5 uncertainty in scale height. Numerical definitions of these atmospheres are given in table I along with the planetary constants used for trajectory calculations.

Figure 2 illustrates boundaries of reference density as a function of scale height for combinations of surface pressure, surface temperature, stratosphere temperature, and mean molecular weight within the limits listed in the figure. Specific heat ratio, γ, has been fixed at 1.40. In the construction of the boundaries, all but one of the basic quantities in the figure were fixed. The remaining quantity was then varied between the limits given. This being done for each of the four basic quantities listed, the final boundary was constructed and encompassed all of the results. The effect of extending the upper limit in surface pressure from 40 to 130 millibars is illustrated by a dashed line. The location of the two atmosphere extremes of

reference 4 (and this study) is denoted by filled symbols as are their corresponding low-pressure (or low density) versions. A discussion of the uncertainty in troposphere structure is omitted in this section, although figure 2 includes the reference density dependence on troposphere structure. It has been noted that in most atmosphere estimates, the tropopause is below that altitude on an entry trajectory where peak deceleration and heating occur. It can therefore be ignored when entry corridors or aerodynamic heating are considered. If landing requirements are of interest, the uncertainty in troposphere structure becomes important. However, in this study the troposphere effects are omitted because they are overshadowed by the upper atmosphere uncertainties.

Composition.- The atmosphere's chemical composition is important in aerodynamic heating calculations. Currently, the composition of the martian atmosphere is uncertain. Except for traces of water vapor, carbon dioxide is the only constituent detected spectroscopically (ref. 7) and estimates of its abundance vary upward from 2 percent. On the basis of the cosmic abundance of elements and the planetary environment of Mars, it is conjectured that the remaining principal constituents are nitrogen and possibly argon, although other gases may be present. However, at the time of this analysis, heat-transfer data were available only in CO_2-N_2 mixtures. Consequently, this study is restricted to investigating the effect of varying the CO_2 abundance relative to N_2, assuming no other constituents.

Entry Corridor

An entry corridor is determined principally by the aerodynamic capabilities of the entering vehicle, the aerodynamic heating and load limits prescribed, and the structure of the upper portion of the atmosphere (i.e., excluding the troposphere). The effects of uncertainties in the structure of the upper atmosphere on entry corridor will be investigated in this section.

The corridor boundaries used in this study are illustrated in figure 3. The "overshoot" bound is that for which the vehicle enters with a constant lift to drag ratio such that lift is directed normal to the trajectory and toward the planet. The aerodynamic drag is just sufficient to decelerate the vehicle to slightly less than parabolic, or capture, speed at exit. The "undershoot" bound is that for which the vehicle enters with a constant outward directed lift to drag ratio such that its maximum deceleration does not exceed 10 earth g (322 ft/sec^2, representative of manned entry limitation).

The entry trajectories can be uniquely defined if the initial trajectory parameters (entry angle, velocity, altitude) and the aerodynamic parameters (L/D, m/C_DA, and their modulation scheme) are known. The trajectory parameters are conveniently expressed in terms of initial velocity ratio ($\bar{V}_i$) and periapsis altitude (h_p) for a fixed initial altitude. The significance of $\bar{V}_i$ lies in the fact that for $\bar{V}_i > \sqrt{2}$, the entry has been initiated at a hyperbolic speed for which aerodynamic braking is required to achieve capture.

In the absence of sufficient braking ($V_{exit} \geq \sqrt{2}$), the vehicle would not return to the planet. Periapsis altitude represents the minimum altitude obtained on the trajectory if no atmosphere or planet surface were encountered. (See fig. 3.) It is in terms of $\bar{V}_i$ and h_p, that the following results are presented.

Scale height effects.- The entry corridor is influenced by both the scale height and reference density, but their effects may be studied separately. Figure 4 illustrates the changes in entry corridor for the two scale height extremes. As noted on the figure, the corridors shown are for a vehicle with aerodynamic parameters; $L/D = \pm 0.5$, and $m/C_DA = 1.0$ slug/ft^2. This selection of aerodynamic parameters is discussed in appendix A along with the result of using other values. All the initial entry conditions are taken at an altitude of 1,000,000 feet above the planet's surface. Although the atmospheres of figure 1 have different reference densities, only the deep atmosphere value was used in comparing the corridors. Using a common value to completely isolate the scale height effects does not alter the conclusions and changes the results only slightly. In figure 4, the corridor for which successful entry is assured, with the scale height uncertainty assumed, lies within the shaded area and is limited in maximum entry velocity.

Reference density effects.- Another reduction in the corridors is imposed by the uncertain reference density. Figure 5 illustrates the effect of both scale height extremes and an order of magnitude reduction in reference density. The figure shows that an order of magnitude reduction in ρ_{ref} causes a downward shift of the entire corridor. The amount of shift depends on scale height as well as reference density. The remaining "usable corridor" is that region not swept by the shifting corridor boundaries and represented in figure 5 by the shaded area.

The dependence of the amount of corridor shift on atmosphere structure can be determined from the analyses of references 8 and 9. That is, for constant values of the aerodynamic parameters, the corridor shift for a change in ρ_{ref} can be shown as:

$$h_p' - h_p \cong H \log_e \frac{\rho'_{ref}}{\rho_{ref}} \tag{1}$$

where the primes denote the new or shifted values.

A corresponding equation for evaluating the influence of changing scale heights was not available in convenient analytical form. However, reference 9 provides a means of evaluating its effects with charts and tables. As seen in equation (1), the effect of uncertain reference density is proportional to scale height as well as $\log(\rho'_{ref})/(\rho_{ref})$. Consequently, the corridor for a low-scale height atmosphere, although shallow is depth, is not reduced by the reference density uncertainty as much as a corridor for larger scale heights. Thus, for the uncertainty in ρ_{ref} considered, the percent reduction in corridor depth is about the same for both scale heights (see fig. 5). For example, the corridor for each scale height extreme is closed at approximately $\bar{V}_i = 4.0$ by the uncertainty in ρ_{ref}.

Combined effects.- If the combined uncertainties in scale height and reference density are now considered, the total effect on entry corridor can be illustrated by superimposing the results of figures 5(a) and (b) and keeping only the unaffected regions. This has been done in figure 6 which shows the remaining corridor (shaded area) to be that of the shallow atmosphere with maximum entry speed limited to $\bar{V}_i < 2.7$. The corridor depth of 10 miles (indicated on the figure) is the minimum guidance capability for a simple system. A comparison of figures 4 and 6 indicates that the uncertainty in scale height limits the entry corridor more than the uncertainty in reference density.

Aerodynamic Heating

Although aerodynamic heating could be analyzed for the corridor limits previously described, the results would be clouded by the effects of lift modulation schemes and deceleration limits. Since the object here is only to illustrate the atmosphere uncertainty effects on heating, this section deals with the simpler problem of nonlifting probe-type vehicles. Consequently, its similarity to the previous section is only that the same uncertainties in atmosphere structures are used.

Aerodynamic heating of a given vehicle shape during entry into an atmosphere depends principally on the vehicle speed, local atmosphere density, and chemical composition. Of the atmosphere structure variables, scale height becomes the only parameter of importance. This is evident when it is realized that, a change in reference density primarily changes only the altitude at which a particular velocity and density combination occurs. The velocity and heating rates at a given density remain unchanged. Reference density does affect the total heating, integrated over the entire trajectory, by altering the total time of flight. However, since terminal heating rates are low compared to the maximum values, the effect is negligible. Therefore the only atmosphere variables treated in this section are scale height and chemical composition. The effects of their uncertainties on both convective and radiative heating are investigated. The heating rates presented refer to stagnation point values only. Estimations of their magnitude contain the assumptions of laminar flow over a cold wall with the stream in thermodynamic equilibrium behind the shock wave. Hence, at best, the results are only qualitative but they sufficiently illustrate the degree to which the atmosphere uncertainties affect aerodynamic heating.

Chemical composition effects.- As discussed in the section on atmosphere uncertainties, the martian atmosphere is believed to contain, as principal constituents, carbon dioxide, nitrogen, and possibly argon. Since heat-transfer data presently available are limited to mixtures of CO_2 and N_2 only, this analysis is likewise limited to those mixtures.

Various investigators have shown (refs. 10 through 14) that both convective and radiative heating rates depend on stream composition. However, they have further demonstrated that for those gas compositions considered here convective heating is relatively insensitive to the gas

composition compared to shock-layer radiation. Therefore, in this study, a single expression independent of gas composition was used for computing convective heating rates. The intent here is to imply only that the composition uncertainty effect on convective heating is small rather than zero but is nevertheless ignored. Reference 10 shows a theoretical 30-percent difference in convective heating rates between pure CO_2 and pure N_2. However, at present these results have not been verified experimentally and a detailed analysis based on them cannot be justified.

Shock-layer radiant intensities measured by James (ref. 11) show nearly an order of magnitude variation in gas mixtures of CO_2-N_2. His results apply only over a limited range of velocities (up to 26,000 ft/sec) but serve to justify the selection of mixture "extremes" in the following manner: figure 7 illustrates the variation of shock-layer radiant intensity with gas mixture, taken from reference 11, and shows intensity is maximum for 7- to 16-percent CO_2. The mixture for peak intensity seems to vary slightly with velocity and density but, in general, the variation is only a few percent. Hence, for this analysis 10-percent CO_2 and 90-percent N_2 is selected as one extreme gas mixture and represents, for all velocities and ambient densities, the mixture for maximum shock-layer radiant intensity. As a lower limit, the radiation heating rates for pure N_2 are used. As seen in figure 7, the difference between pure CO_2 and pure N_2 intensity is not large for the higher speeds. In addition, a low CO_2 concentration in the Mars atmosphere is favored by most authors, making pure N_2 appear as a more sensible "other extreme."

For radiation data at velocities higher than those of James, the investigations of Gruszczynski and Warren (ref. 12) were used. They measured shock-layer radiation intensities in CO_2-N_2 mixtures up to 25-percent CO_2 and at velocities between 30,000 and 45,000 fps. Their results show very slight or no dependence on gas mixture. This lack of composition dependence in the higher velocity data compared to those below 26,000 fps is attributed to dissociation of the principal radiators at the higher velocities.

In order to make the heating-rate calculations necessary for this analysis, equations in terms of ambient density and vehicle speed were empirically fitted to the data of references 11 and 12. The origin of these equations and appropriate constants for the gas mixtures used are given in appendix B. As an example of the results, radiant heating rates for the two composition extremes are illustrated in figure 8 for a single ambient density. As the figure indicates, the dependence of radiative heating on gas compositions begins to diminish as velocities approach 30,000 fps and disappears altogether at higher velocities. Reference 12 provides a more complete discussion of this phenomenon and includes some more precise theoretical examples.

Results of heating calculations showing composition effects.- The effect on maximum stagnation point heating rate of varying composition between the established extremes is presented in figure 9(a). The results apply to a zero lift, 90° entry into the shallow atmosphere where the composition effects are most pronounced. A 90° entry into the shallow atmosphere yields the highest heating rates of any nonlifting entry for a given entry speed.

Consequently, any differences in heating rate due to atmosphere composition or structure variation will be most evident. Maximum values of the sum of convective and radiative heating rates achieved on the trajectory are plotted in figure 9(a) as a function of the initial entry velocity.[1] The convective contribution is shown by the shaded area. As the figure indicates, the entry velocity at which radiation becomes significant is strongly dependent on the gas composition. The same results would appear for entry into a deeper atmosphere but with less effect of the composition uncertainty. In addition, in the deeper atmosphere the entry velocities at which radiation becomes significant for either mixture would increase. It is interesting to note that at entry velocities where the speed at maximum heating is in excess of approximately 30,000 fps (i.e., $V_i \approx 40{,}000$ fps) the composition dependence shown in figure 9(a) disappears; that is, the curves of figure 9(a) for both mixtures merge to a single value due to the heating-rate behavior shown by figure 8.

If the stagnation point heating rate is integrated with respect to time over the entire trajectory, the result is the "total heat" which must be absorbed or dissipated at the stagnation point. The effect of composition uncertainty on heat-shield size and weight is implied by its effect on "total heat." Figure 9(b) presents the dependence of total heat on gas composition for the same trajectories used in computing the results of figure 9(a). As can be seen, the conclusions drawn from figure 9(a) also apply here. Only a slight difference between the results of figures 9(a) and 9(b) exist in that for 9(b) the curves for each mixture do not completely merge at the higher speeds. This is a result of the differences in the integrated radiation at speeds below those of maximum heating rate.

From the preceding analysis, it can be concluded that for entry speeds greater than 20,000 fps, the uncertainty in chemical composition of the martian atmosphere may impose a significant uncertainty in the amount of radiative heating received by the entering vehicle - hence in the heat-shield design.

Atmosphere structure effects.- As previously discussed, scale height is the atmosphere structure parameter of significance with regard to aerodynamic heating. An example of its effect is given by figure 10(a) which illustrates the effect of scale height uncertainty on maximum stagnation point heating rate. The heating rates presented are again for a 90°, zero-lift entry into the "deep" and "shallow" atmospheres of figure 1 assuming a single composition of 90-percent N_2 and 10-percent CO_2. Both the convective and radiative components are included with the convective contribution given by the shaded regions. The dependence of heating rate on scale height given by the figure can be verified in the following manner. As shown in equation (B5), the heating rates vary directly as $\rho_\infty{}^n$ where n is an exponent depending on the type of heating (convective or radiative) and the speed range ($n = 0.5$ for convective heating, and 1.3 to 1.6 for radiative). By the analysis of reference 15, the density at maximum heating can be expressed as:

[1] It is recognized that the maximums of $\dot{q}_c$ and $\dot{q}_r$ do not occur at precisely the same point on a trajectory. However, for the purposes of this study, their sum is assumed to represent the maximum total heating rate.

$$(\rho_\infty)_{\max \dot{q}} \sim \frac{m/C_D A \sin \varphi_i}{H} \qquad (2)$$

thus describing the dependence of density at maximum heating not only on scale height (H) but on $m/C_D A$ and initial flight-path angle (φ_i) as well. The trends of figure 10(a) follow these relations by showing the individual heating rates (i.e., $\dot{q}_c$ and $\dot{q}_r$) proportional to $(1/H)^n$ [i.e., $q \sim (\rho_\infty)^n_{\max \dot{q}} \sim (1/H)^n$]. As seen in the figure, and by equation (2), the radiative heating rates show a more pronounced effect of the scale height uncertainty than convection due to the value of n. Thus the heating-rate uncertainty is magnified when radiation becomes prevalent. In general terms, it can be said that the effect of scale height uncertainty on heating rate is to alter the entry velocity at which radiation will be significant and to vary the rate at a given velocity by a large factor depending on the velocity.

The total heat, as affected by scale height uncertainty, is illustrated by figure 10(b). The values plotted are for the same conditions as figure 10(a) and the same scale height extremes. Again, the contribution due to convection is denoted by the shaded regions. The figure shows that convective heating varies directly with scale height while the radiative heating varies inversely. The opposite behavior for the two types of heating is due to the value of n. In the integration of $\dot{q}$ over the trajectory, H remains in the denominator of the integral for n greater than 1.0 (radiation) but appears in the numerator for n less than 1.0 (convection). The net result is that total heating shows only a weak dependence on scale height with the degree determined by entry speed for a given vehicle. This weak dependence exists in general for all similar values of vehicle nose radius, $m/C_D A$, entry angle, and other gas compositions.

The Landing Problem

Another problem of prime importance in planetary entry is that of controlling the terminal portion of the trajectory and/or landing the vehicle. An entry vehicle design can sometimes be more restricted by the trajectory terminal requirements than any other consideration. This is particularly true in the case of Mars where a low surface pressure makes deceleration to velocities appropriate for soft landing difficult. The role of the atmosphere uncertainties is to further increase the difficulties by forcing the vehicle designer to choose the lowest pressure estimate as the design atmosphere. If such considerations as altitude at parachute deployment speed or impact velocity are important, the entry vehicle design becomes critical. As an example, it is instructive to examine the altitude at which a nonlifting and unmanned vehicle of given $m/C_D A$ would decelerate to some "parachute deployment" speed. Figure 11 provides plots of altitude as a function of atmosphere pressure for the two greatest extremes of figure 1 (deep atmosphere and the low pressure extreme of minimum scale height) plus two atmospheres with a surfaces pressure of 40 mb. At the top of figure 11 are plots of $m/C_D A$, again as a function of atmosphere pressure. The values

plotted are for a vertical entry angle and over a wide range of the ratio of entry velocity to parachute deployment velocity. It can be seen that by combining the two parts of figure 11, a direct correlation is made between m/C_DA and the altitude at which a given parachute deployment speed will be achieved.

Several conclusions can be drawn from figure 11:

(a) It is evident that the choice of m/C_DA is influenced by atmosphere structure, parachute deployment speed, and altitude, and entry velocity. However, for a particular deployment altitude, the effect of entry and deployment speeds on required m/C_DA is small compared to that of atmosphere structure. Therefore, the following conclusions may be generally applied for all speeds of current interest.

(b) The altitude at which a vehicle of given m/C_DA will reach parachute deployment speed is extremely uncertain due to the atmosphere structure uncertainty. This can be seen from the figure for one of the examples of constant m/C_DA indicated. For example, altitude can vary from zero to 80,000 ft for an $m/C_DA = 0.4$ and surface pressure between 10 and 40 millibars.

(c) Finally, of prime significance, the development of an entry vehicle which is certain to reach parachute deployment speeds for altitudes above 20,000 ft appears to be exceptionally difficult. This is based on the assumption that a minimum practical value of m/C_DA is 0.2 slug/ft^2 and that the design atmosphere must be the low-pressure extreme shown by figure 11. Lower m/C_DA values can be shown to require extremely efficient structural design possibly beyond modern design capability.

In addition, an m/C_DA greater than 0.4 slug/ft^2 may result in surface impact before the parachute is deployed. It therefore appears that for the minimum pressure atmosphere assumed in this study, the design of a first generation Mars entry capsule, requiring soft landing, is restricted to the very limiting m/C_DA values between 0.2 and 0.4 slug/ft^2.

In general terms, it can be concluded that the effects of a low surface pressure on vehicle design are augmented to a significant degree by the atmosphere structure uncertainty. If the atmosphere is, in fact, the low pressure extreme, the density structure from the surface to several hundred thousand feet must be defined before entry experiments can be assured of success.

CONCLUDING REMARKS

The purpose of this study has been to provide a general evaluation of the degree to which the uncertainties in structure and composition of the martian atmosphere affect various aspects of entry. The illustrations and analysis employed are clearly of an approximate nature. However, the results

show the need for better definition of the atmosphere. In particular, the following is a summary of the results derived, based on the specified limits of atmosphere structure and chemical composition.

(a) The usable entry corridor for manned flight is reduced considerably by uncertainties in the atmosphere structure; particularly by the uncertainties in scale height.

(b) Aerodynamic heating predictions for an unmanned probe cannot establish whether the heating rates experienced for a given entry velocity will include large amounts of shock-layer radiant heating or not because of the uncertainty in both composition and structure of the atmosphere.

(c) The problem of soft landing a probe is perhaps the most critical. Low surface pressures tax the vehicle design by requiring a high drag, low weight vehicle to insure adequate aerodynamic deceleration. The uncertainties in surface pressure could result in a probe of excessively limited payload.

Ames Research Center
National Aeronautics and Space Administration
Moffett Field, Calif., Sept. 23, 1964

APPENDIX A

THE EFFECT OF USING OTHER AERODYNAMIC PARAMETERS ON THE RESULTS PERTAINING TO ENTRY CORRIDORS

In order to verify the validity of the conclusions drawn from the section on entry corridors where a single set of aerodynamic parameters was used ($L/D = \pm 0.5$, $m/C_DA = 1.0$), this appendix seeks to illustrate the consequences of changing these parameters to other common values.

LIFT-TO-DRAG RATIO

Since the existence of an entry corridor implies a manned entry (maximum deceleration limits usually are not necessary for a probe), it is likely that a lifting vehicle will also be used. The advantages lie in the ability of lift to increase the corridor depth and allow a landing site selection. Hence, the zero lift corridors may be ruled out a priori as poor examples for manned entry studies even though the atmosphere uncertainties penalize them to a much greater extent. Furthermore, values of L/D greater than 1/2 do not provide an appreciable advantage over those near 1/2. This can be realized from figure 12. Plotted there are the corridor depths (Δhp) as a function of lift-to-drag ratio. Values are given for two atmospheres and two entry velocities. For $L/D = \pm 1/2$, they agree with the corridor depths of figure 4. As shown, the greatest gain in corridor depth with increasing L/D occurs between $L/D = 0$ and $\pm 1/2$. Increasing L/D further will tax the vehicle design and improve its capability only slightly. Hence, L/D values of $\pm 1/2$ were selected as representative of a manned entry vehicle and the conclusions obtained using them are qualitatively correct for all lifting entries. As an indication of how the entry corridor results would be affected by using other values of L/D, it is obvious from figure 12 that a lower L/D would reduce the corridor depth. This coupled with the corridor shift due to ρ_{ref} uncertainty could close the usable corridor, shown in figure 6, toward zero. Higher L/D's would, of course, tend to improve the situation.

m/C_DA EFFECTS

Current values of m/C_DA used for analyzing Mars entry vehicles have been both higher and lower than that chosen for the section on entry corridors. For a manned entry vehicle, however, $m/C_DA = 1.0$ slug/ft^2 appears to be a representative value. The effect of changing m/C_DA is very similar to that of changing reference density. The entire corridor is shifted without altering the corridor depth. From the analysis of reference 9, the amount of shift for a given scale height and reference density can be shown as:

$$h_p' - h_p \cong -H \log_e \frac{(m/C_DA)'}{(m/C_DA)} \qquad (A1)$$

where the primes denote the new or shifted values.[1] In figure 13 equation (A1) is applied to the scale heights of figure 1. As can be seen, the effect on corridor position with other values of m/C_DA is relatively small compared to the atmosphere uncertainty effects or use of other L/D values. Thus, the selection of $m/C_DA = 1.0$ slug/ft^2 for this study, although representative, is inconsequential, and the results apply qualitatively to all types of manned vehicles.

[1]The right side of equation (A1) can be added directly to equation (1). The result then gives the dependence of the corridor levels on both ρ_{ref} and m/C_DA for a given scale height.

APPENDIX B

EQUATIONS FOR COMPUTING STAGNATION-POINT HEATING RATES

Since the heating rate may be divided into contributions of convection and shock-layer radiation, this description will be similarly divided. The intent here is not to provide a rigorous derivation of the heating equations, but only to define the approximations used in the calculations for this study. In all cases the following assumptions are made:

(a) The flow in the vicinity of the stagnation point is laminar and in complete thermodynamic equilibrium.

(b) The exposed surface is a cold wall.

(c) The vehicle has a hemispherical nose.

(d) Only order-of-magnitude effects are considered.

Based on the above, the following equations were devised.

CONVECTIVE HEATING

As discussed in the text under "aerodynamic heating," convective heating is relatively insensitive to gas composition in CO_2-N_2 mixtures. For mixtures containing 0- to 10-percent CO_2, references 10 and 12 show convective heating rates to be well represented by:

$$\dot{q}_c\sqrt{R_N} = 8.7\times10^{-4}p_s^{1/2}(h_s - h_w)$$

Assuming

$$p_s \cong \rho_\infty V_\infty^2$$

and

$$h_s - h_w \cong \frac{V_\infty^2}{2\bar{g}J}$$

we have the following result:

$$\dot{q}_c\sqrt{R_N} = 1.7\times10^{-8}\rho_\infty^{1/2}V_\infty^3 \qquad \text{(B1)}$$

Equation (B1) was used for all the convective heating calculations.

RADIATIVE HEATING

As shown by many investigators (e.g., ref. 14), stagnation-point radiative heating can be expressed as:

$$\dot{q}_r = \frac{1}{2} I_s \delta_s$$

where the shock wave stand-off distance (δ_s) for a hemispherical nose can be approximated by $\delta_s = 0.805 R_N(\rho_\infty/\rho_s)$ (ref. 16) for most gases of interest.

Combining expressions, we have:

$$\frac{\dot{q}_r}{R_N} = 0.805 \frac{\rho_\infty}{\rho_s} I_s \tag{B2}$$

The problem remains then of writing $(\rho_\infty/\rho_s)I_s$ in terms of ρ_∞ and V_∞, the known parameters in an entry trajectory calculation. To approximate the ratio ρ_∞/ρ_s for the crude accuracy needed here, it was found satisfactory to write:

$$\frac{\rho_\infty}{\rho_s} = A\rho_\infty{}^a V_\infty{}^b \tag{B3}$$

where the constants A, a, b depend on the composition and speed range of interest. Values of radiant intensity (I_s) can also be expressed by a similar equation for a given composition and speed range; that is,

$$I_s = C\rho_\infty{}^M V_\infty{}^N \tag{B4}$$

where C, M, and N are again constants. The data of references 12 and 17 were fitted to equation (B3) and the data of references 11, 12, and 18 to equation (B4) to determine the corresponding constants for each gas mixture and speed range. Substitution of equations (B3) and (B4) were then substituted into equation (B2) with their appropriate constants to yield the following representation of radiant heating at the stagnation point:

$$\frac{\dot{q}_r}{R_N} = K\left(\frac{\rho_\infty}{\rho_{SL_\oplus}}\right)^n \left(\frac{V_\infty}{10^4}\right)^m \tag{B5}$$

where the constants, K, n, and m are given by the following table:

Velocity range	Mixture percent CO_2	K	n	m
Less than 30,000 fps	0	427	1.63	6.4
	10	3714	1.34	6.4
30,000 to 45,000 fps	All mixtures	0.006	1.54	17.0

Several qualifications concerning equation (B5) and the table of constants must be made.

(a) The number of significant figures included in the table is not an indication of accuracy.

(b) The speed range indicated for each set of constants is only approximate (e.g., see fig. 8). For a given mixture the intersection of the curves for heating rates corresponding to each speed range varies with density. The set of constants giving the highest value of $\dot{q}_r$ for a given mixture, density, and velocity were used.

REFERENCES

1. Spiegel, Joseph M.: Effects of Mars Atmospheric Uncertainties on Entry Vehicle Design. IAS Paper 62-96.

2. Adams, M. C., Georgiev, S., Levine, P., and John, R. R.: Some Recent Studies of New Re-Entry Problems. AIAA Paper 63-476.

3. Peterson, Victor L., and Tobak, Murray: Theory of the Tumbling and Subsequent Large-Amplitude Oscillations of Vehicles Entering Planetary Atmospheres. Proceedings of the Aerospace Forum I Session, IAS 31st Annual Meeting, N. Y., S.M.F. Fund Paper FF-34, Jan. 1963, pp. 74-81.

4. Schilling, G. F.: Limiting Model Atmospheres of Mars. R-402-JPL, The Rand Corp., Aug. 1962.

5. Kellogg, William W., and Sagan, Carl: The Atmospheres of Mars and Venus. Publication 944, National Academy of Sciences, National Research Council, 1961.

6. Kaplan, L. D., Münch, G., and Spinrad, H.: An Analysis of the Spectrum of Mars. The Astrophysical Jour., vol. 139, no. 1, Jan. 1964, pp. pp. 1-15.

7. Rasool, S. I.: Structure of Planetary Atmospheres. AIAA Jour., vol. 1, no. 1, Jan. 1963, pp. 6-19.

8. Loh, W. H. T.: Dynamics and Thermodynamics of Planetary Entry. Prentice-Hall, Inc., Englewood Cliffs, N. J., 1963.

9. Chapman, Dean R.: An Analysis of the Corridor and Guidance Requirements for Supercircular Entry Into Planetary Atmospheres. NASA TR R-55, 1960.

10. Scala, S. M., and Gilbert, L. M.: Theory of Hypersonic Laminar Stagnation Region Heat Transfer in Dissociating Gases. R63SD40 General Electric, 1963.

11. James, Carlton S.: Experimental Study of Radiative Transport From Hot Gases Simulating in Composition the Atmospheres of Mars and Venus. AIAA Paper 63-455.

12. Gruszczynski, J. S., and Warren, W. R., Jr.: Experimental Heat Transfer Studies of Hypervelocity Flight in Planetary Atmospheres. AIAA Paper 63-450.

13. Seiff, Alvin: Atmosphere Entry Problems of Manned Interplanetary Flight. AIAA Technical Papers Volume CP-4, Proc. AIAA Meeting on Engineering Problems of Manned Interplanetary Exploration, Palo Alto, Calif., Sept. 30-Oct. 1, 1963, pp. 19-33.

14. Demele, Frederick A.: A Study of Convective and Radiative Heating of Shapes Entering the Atmosphere of Venus and Mars at Superorbital Speeds. NASA TN D-2064, 1963.

15. Allen, H. Julian, and Eggers, A. J., Jr.: A Study of the Motion and Aerodynamic Heating of Ballistic Missiles Entering the Earth's Atmosphere at High Supersonic Speeds. NACA Rep. 1381, 1958.

16. Seiff, Alvin: Recent Information on Hypersonic Flow Fields. NASA SP-24, 1962, pp. 19-32.

17. Ziemer, Richard W.: Extended Hypervelocity Gas Dynamic Charts for Equilibrium Air. STL/TR-60-0000-09093, Space Tech. Lab., Inc., April 1960.

18. Page, William A.: Shock-Layer Radiation of Blunt Bodies Traveling at Lunar Return Entry Velocities. IAS Paper 63-41.

TABLE I.- ATMOSPHERE AND PLANETARY CONSTANTS USED FOR THIS ANALYSIS

(a) Atmosphere structure constants[1]

Atmosphere according to figure 1	H, ft	ρ_{ref}, slugs/ft^3	ρ_{surf}, slugs/ft^3	Tropopause altitude, ft	Surface pressure, mb	Surface temperature, ^{o}R	Reference
Deep	65,000	3.412×10^{-4}	2.891×10^{-4}	32,810	132.6	540	4
Shallow	25,590	7.852×10^{-4}	1.436×10^{-4}	83,500	41.04	360	4
Low pressure	(2)	(2)	same as ρ_{ref}	0	11	undefined	5

[1]Number of digits supplied in this table is not an implication of the accuracy. Also, the values listed are those used for calculations in this report and are not precise quotations of the references associated with them.

[2]Low pressure atmospheres are of identical scale heights with an order of magnitude lower value of ρ_{ref}.

(b) Planetary constants

Mean radius	11.09×10^{6} ft
Gravitational parameter, $\mu = gr^2$	1.5152×10^{15} ft^3/sec^2
Circular velocity at 1,000,000 ft altitude	11,200 ft/sec
Mean acceleration due to gravity at the surface	12.3 ft/sec^2

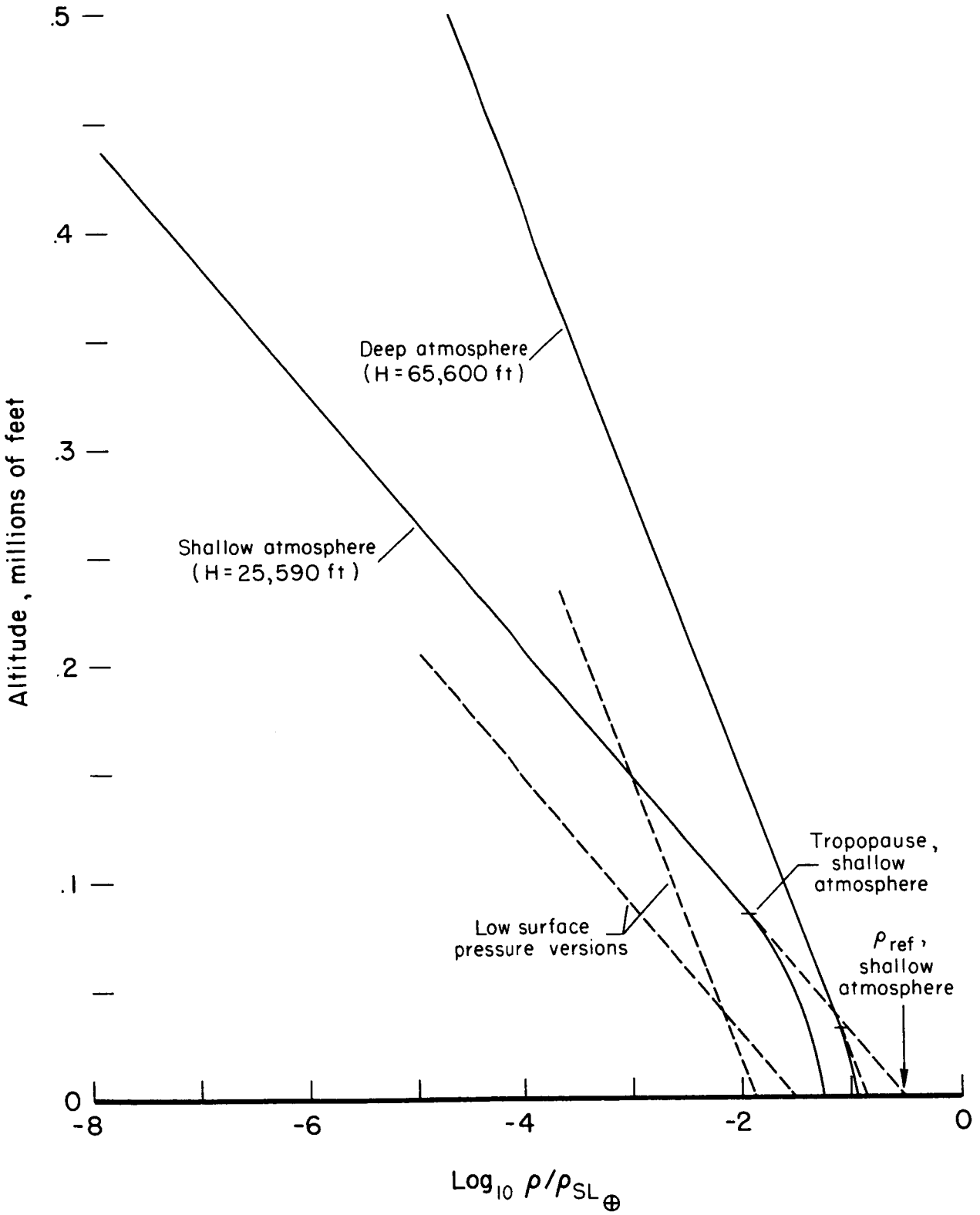

Figure 1.- Assumed extreme model atmospheres for Mars.

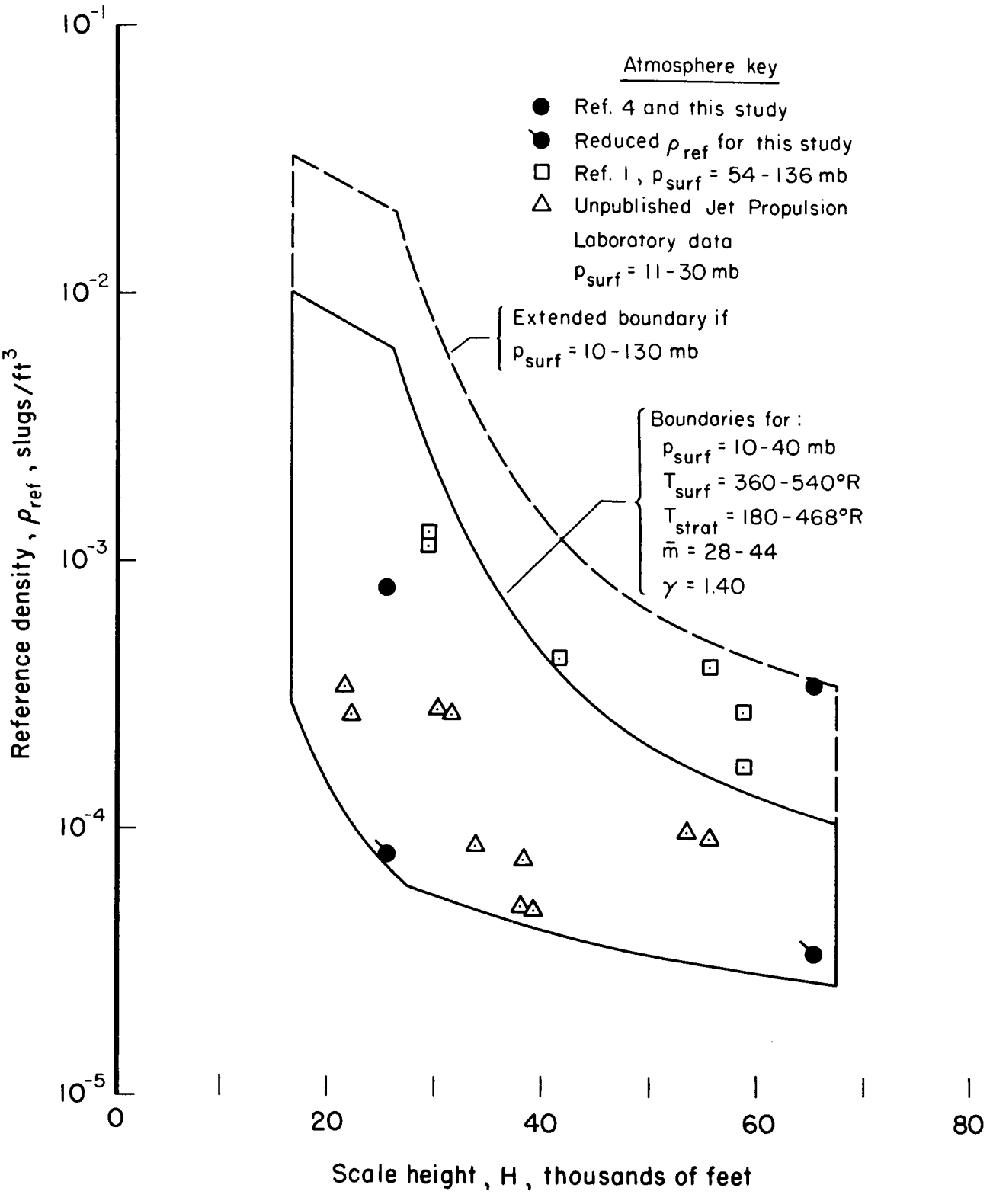

Figure 2.- Mars atmosphere limits.

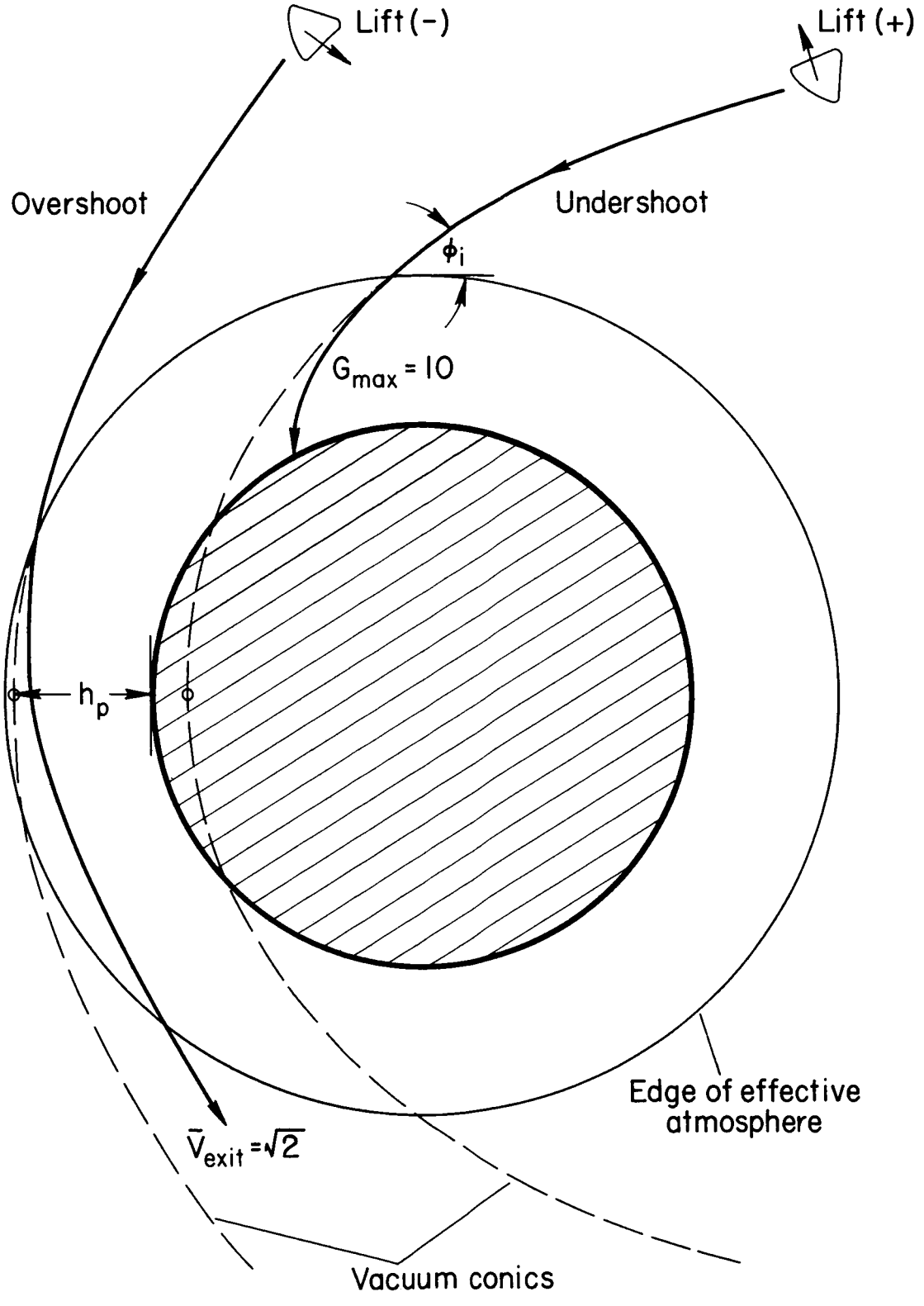

Figure 3.- Entry corridor boundaries.

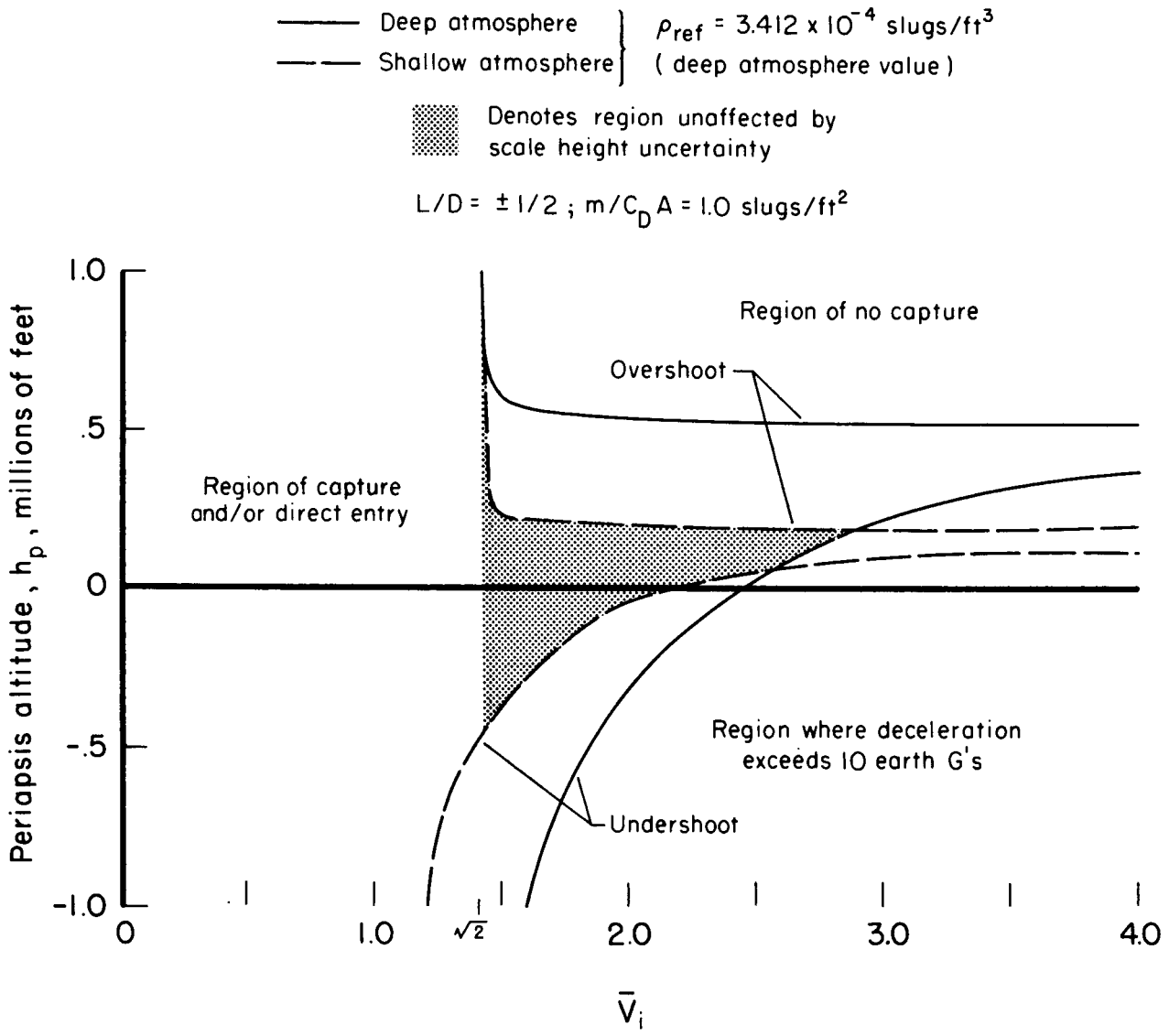

Figure 4.- Scale height effect on entry corridor.

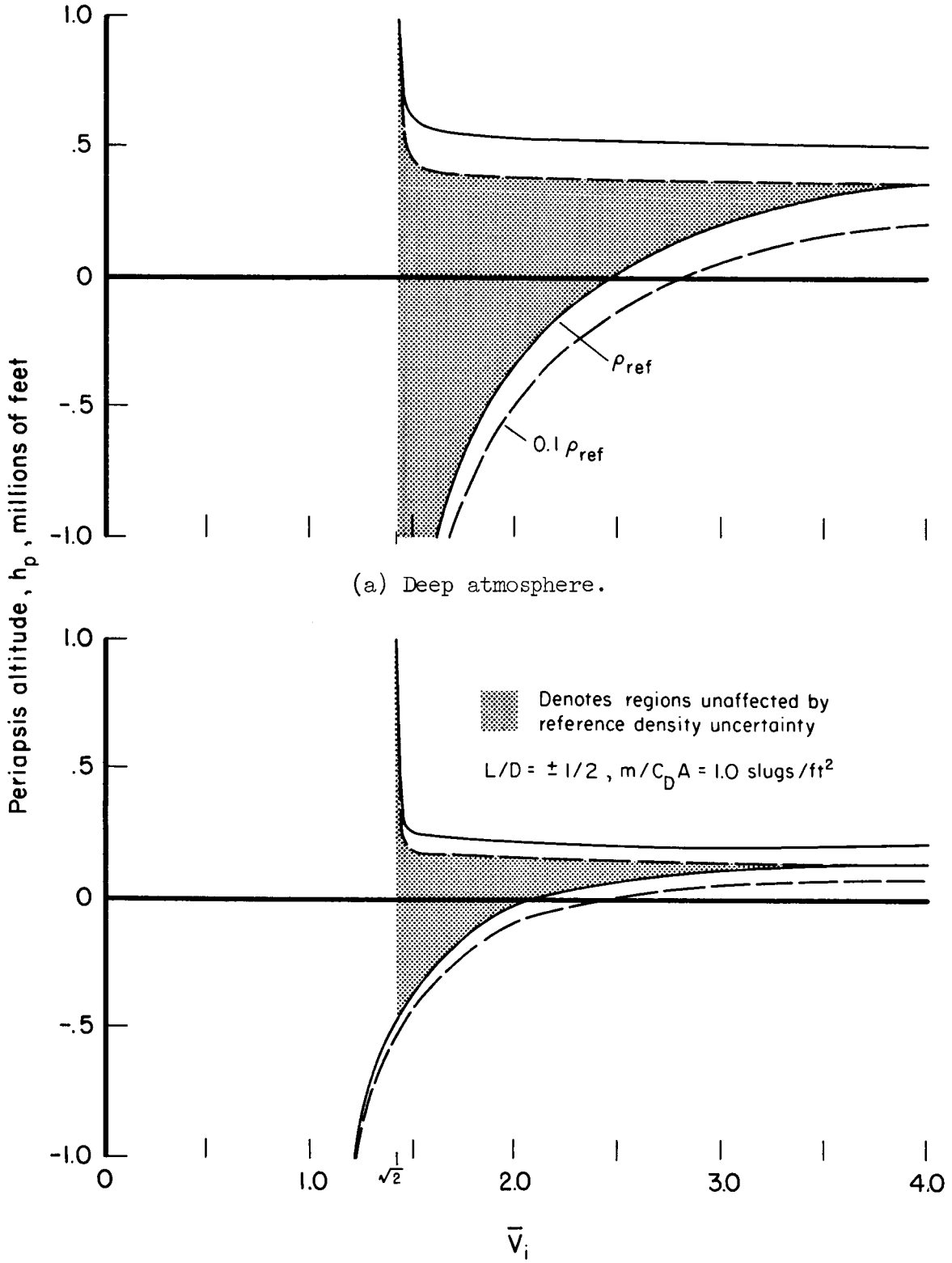

(a) Deep atmosphere.

(b) Shallow atmosphere.

Figure 5.- Reference density effect on entry corridor.

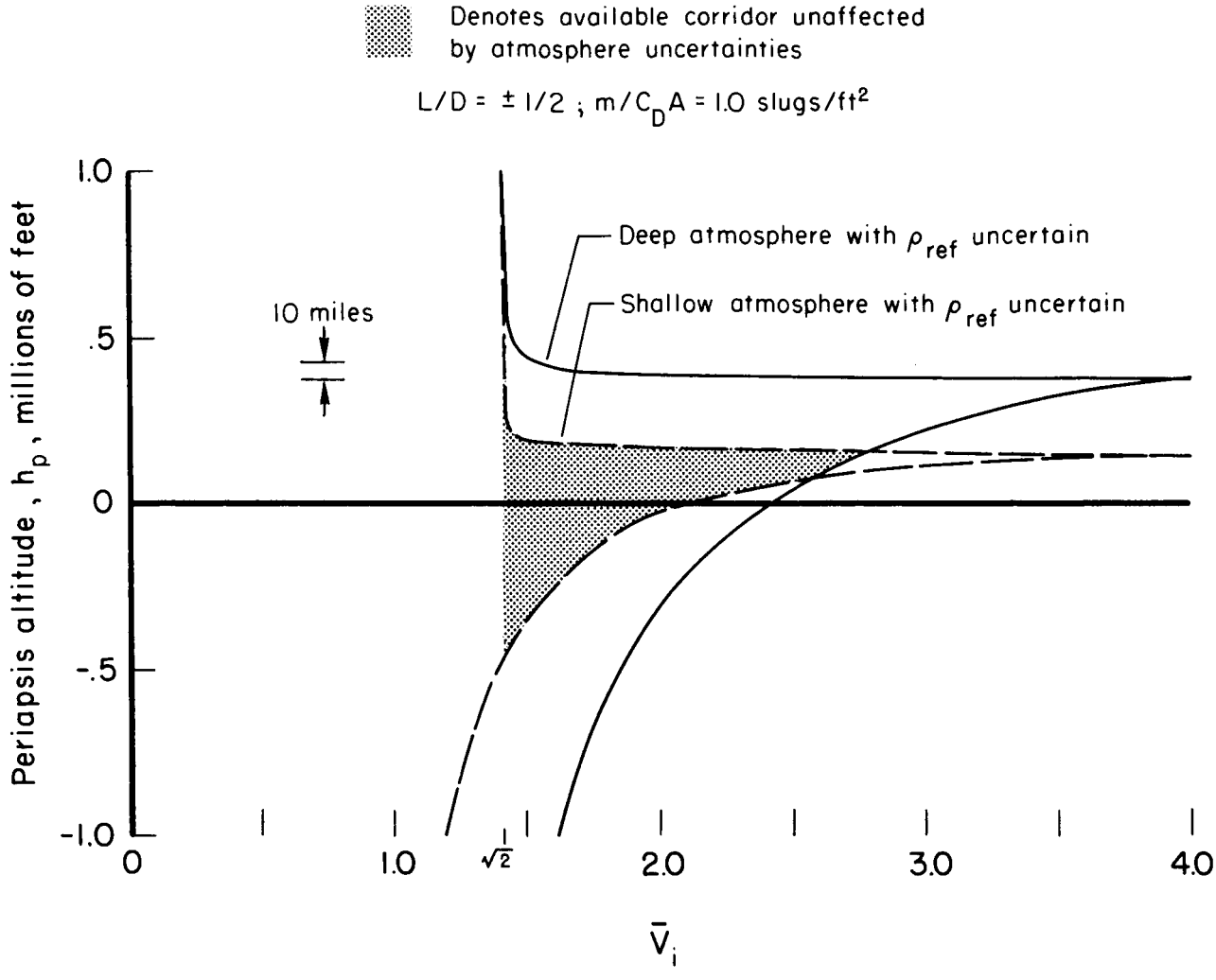

Figure 6.- Combined atmosphere uncertainty effects on entry corridor.

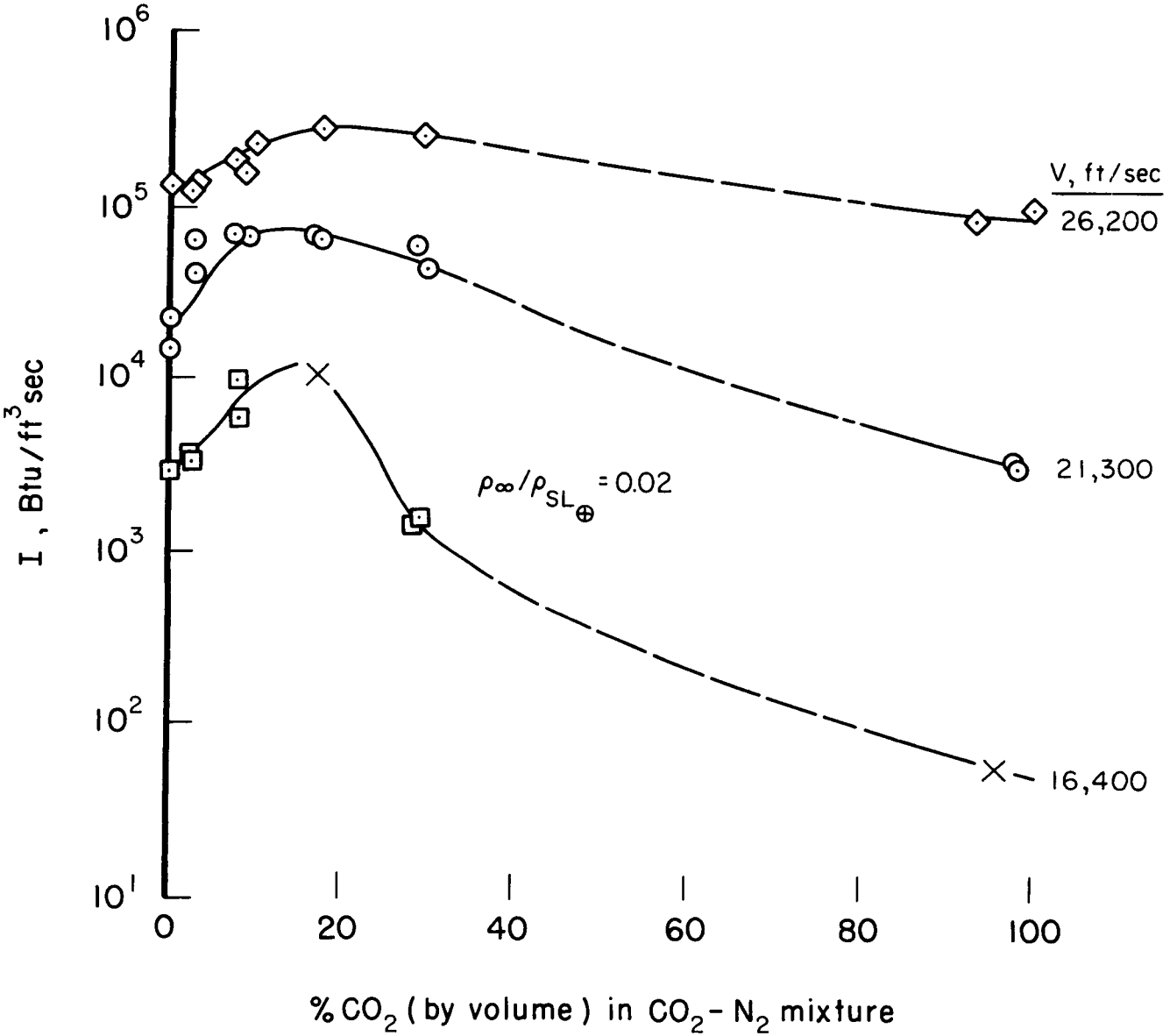

Figure 7.- Effect of CO_2 concentration on total radiation (ref. 11).

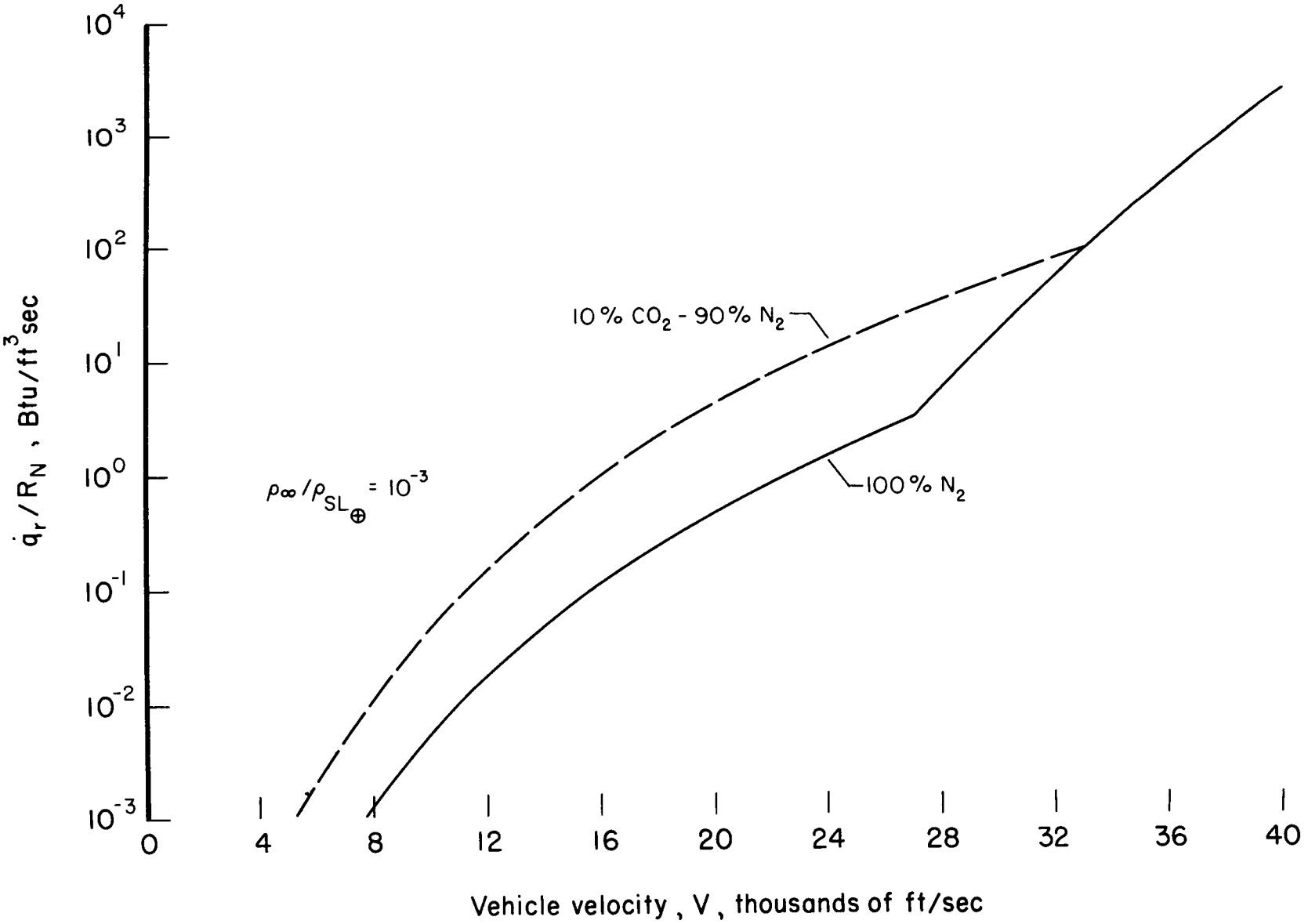

Figure 8.- Stagnation point radiative heating rate approximations (eq. (B5)).

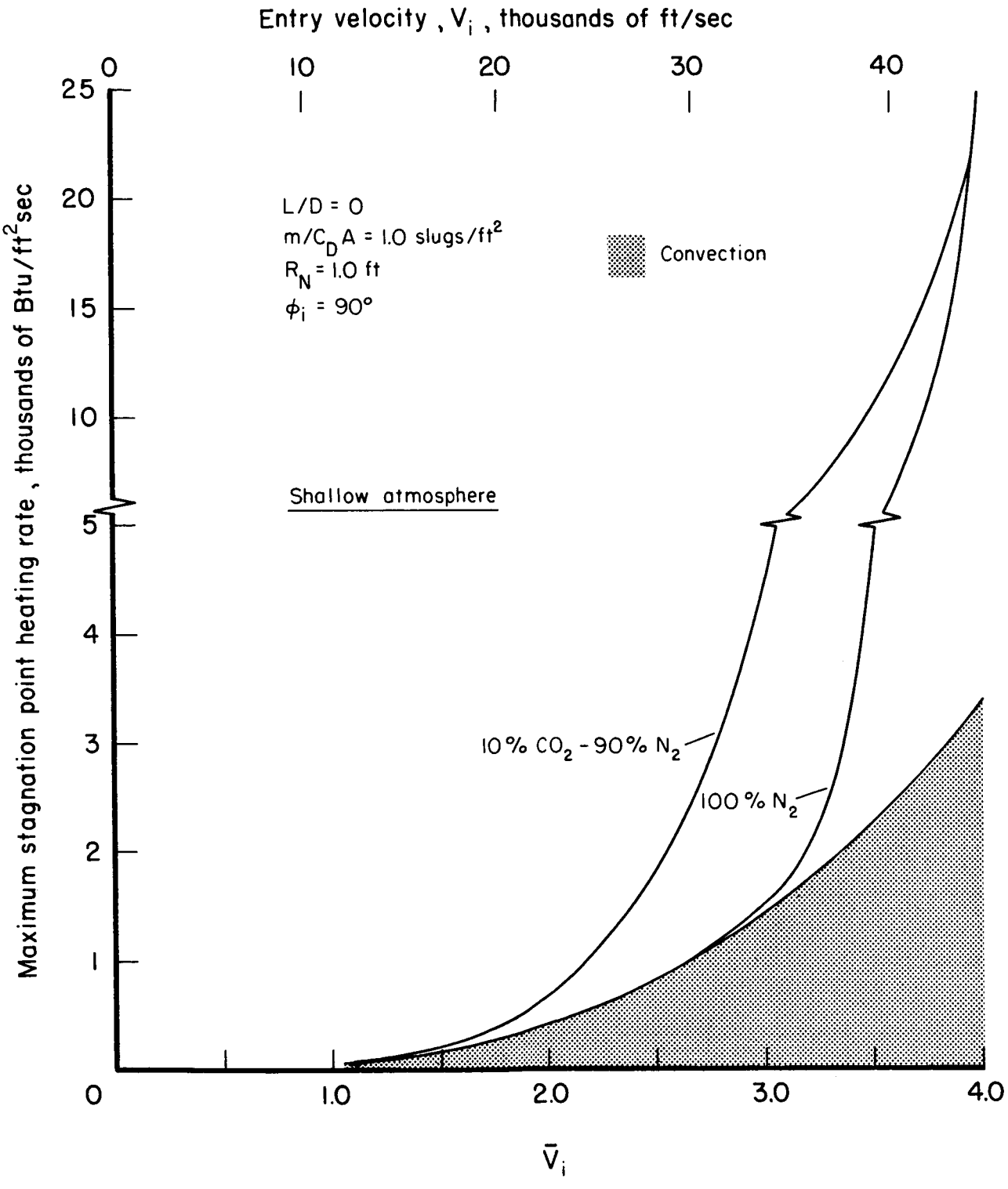

(a) Heating rate.

Figure 9.- Atmosphere composition effect on stagnation point heating.

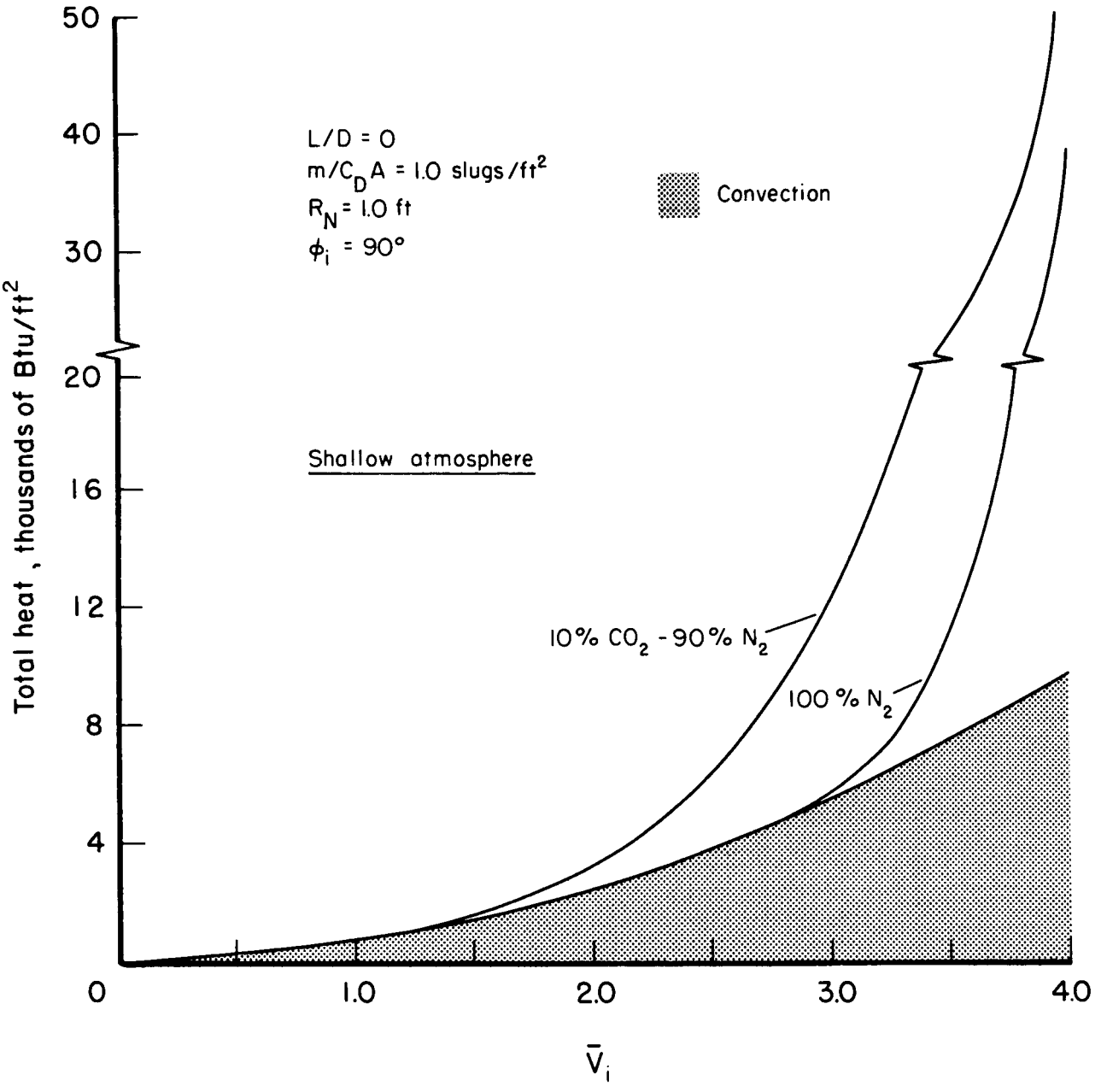

(b) Total heat.

Figure 9.- Concluded.

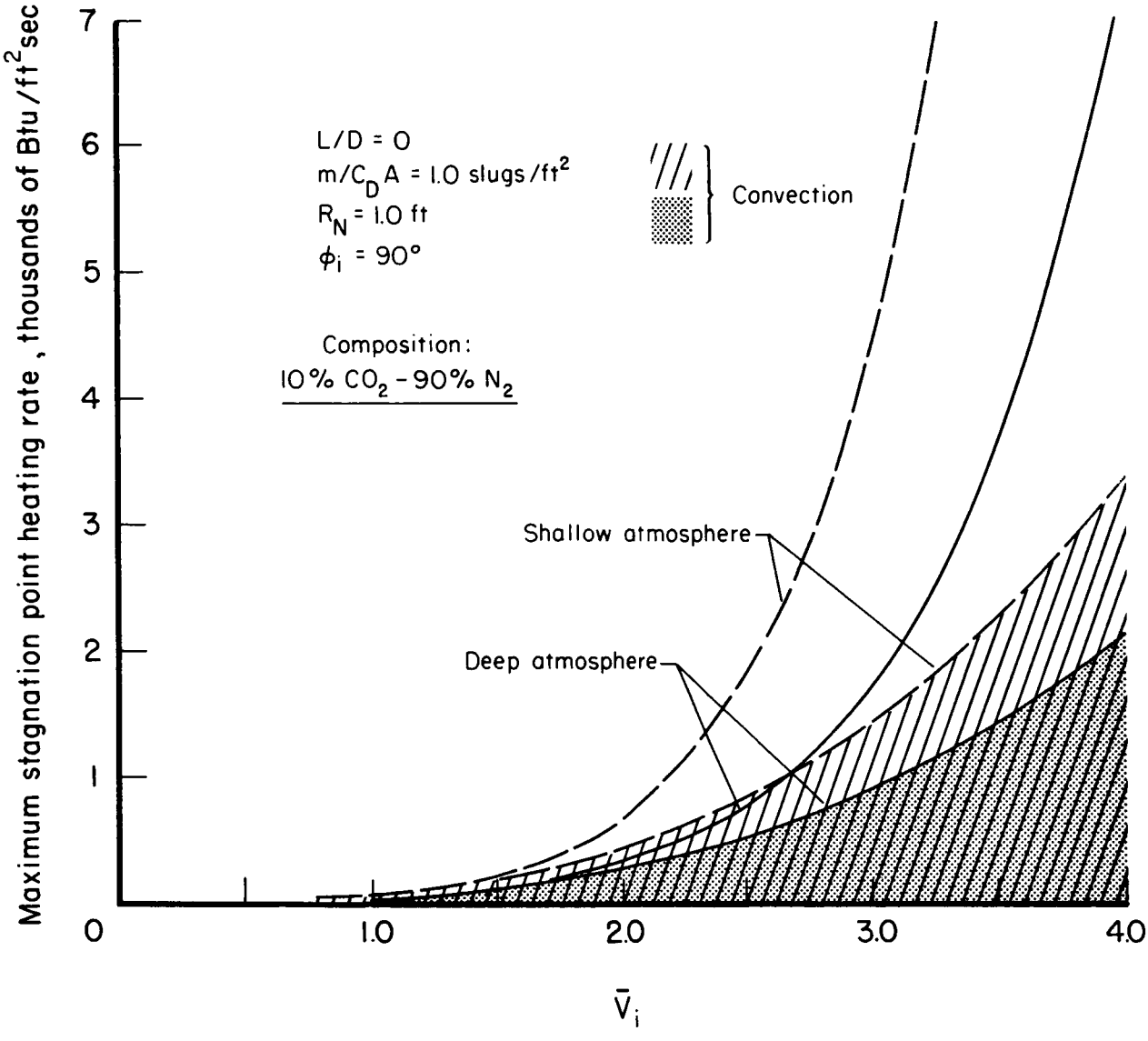

(a) Heating rate.

Figure 10.- Scale height effect on stagnation point heating.

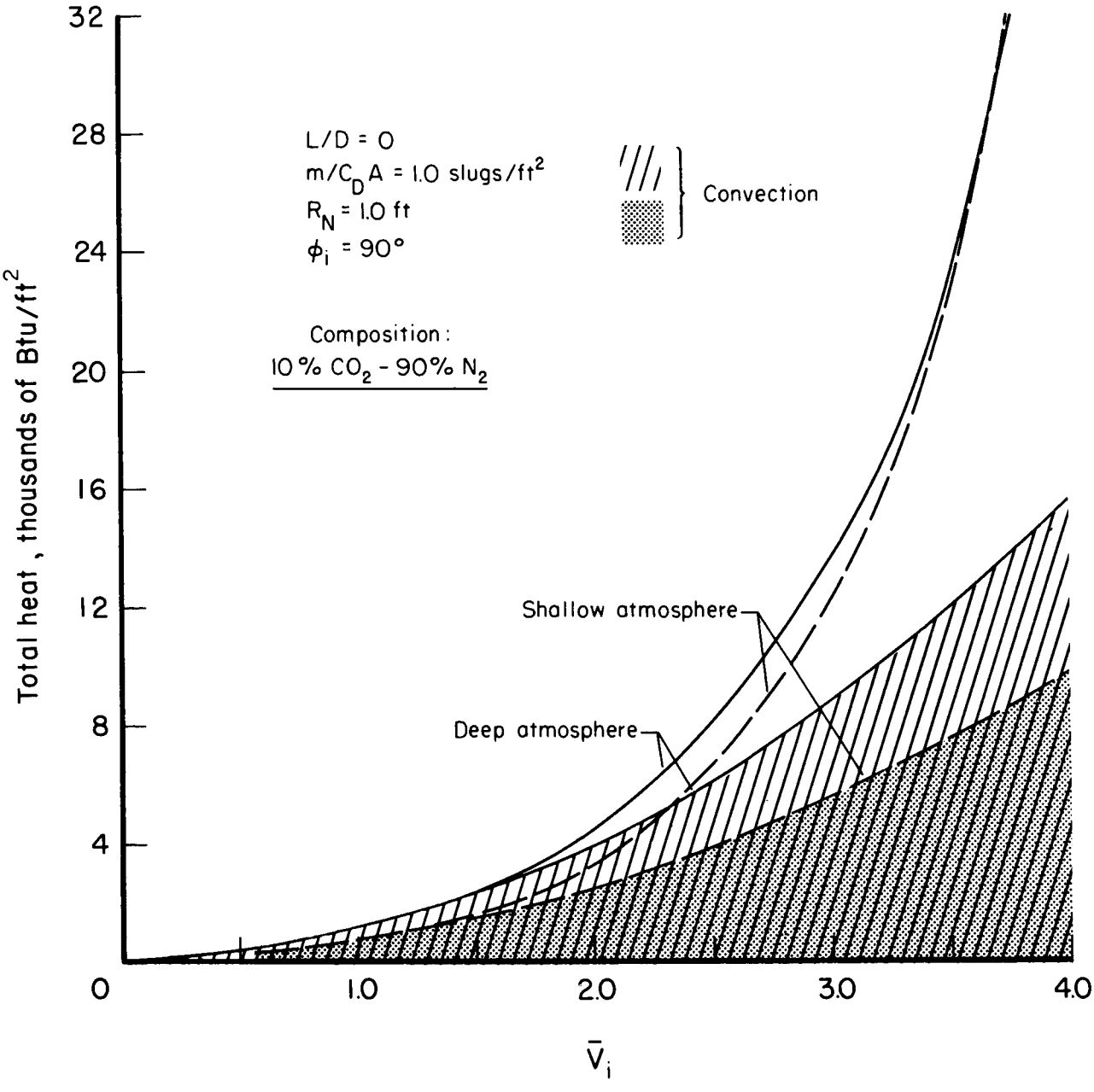

(b) Total heat.

Figure 10.- Concluded.

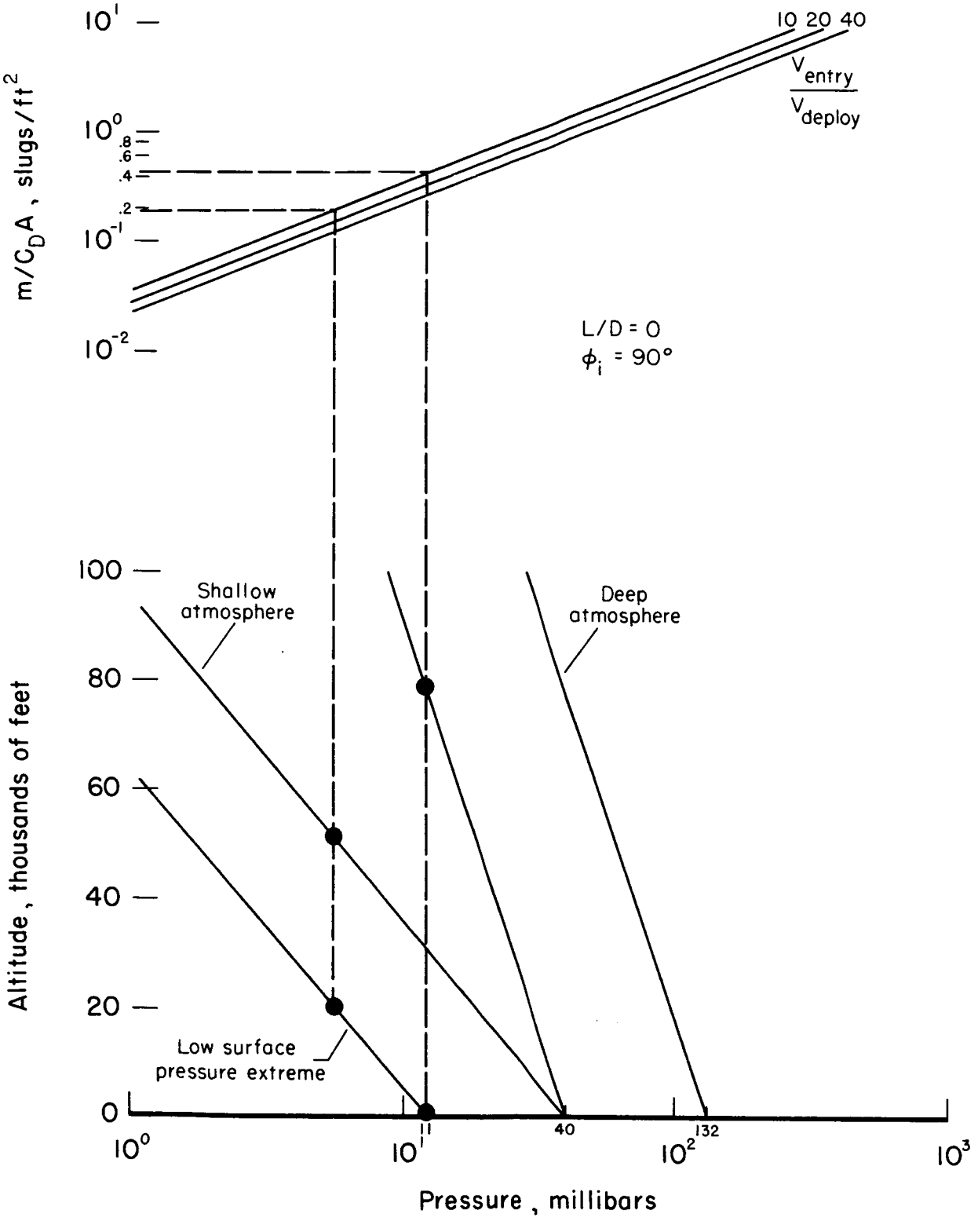

Figure 11.- Effect of atmosphere uncertainty on vehicle landing.

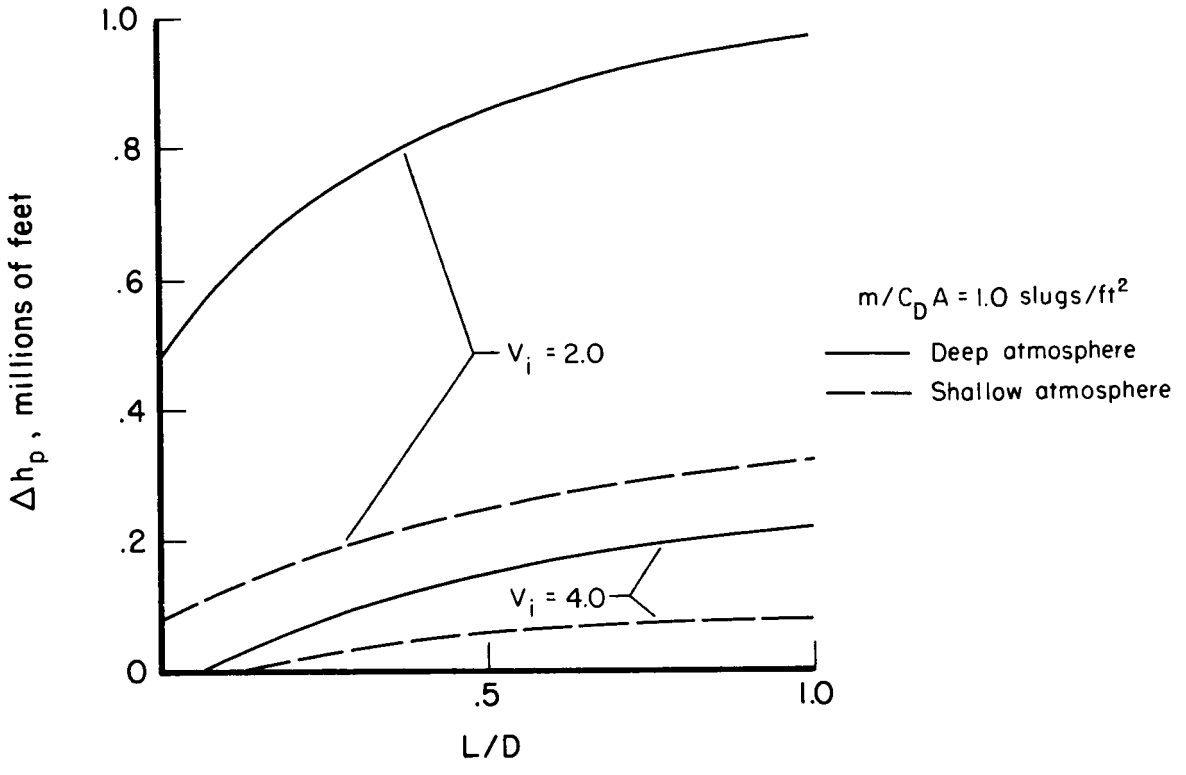

Figure 12.- Effect of lift on corridor depth.

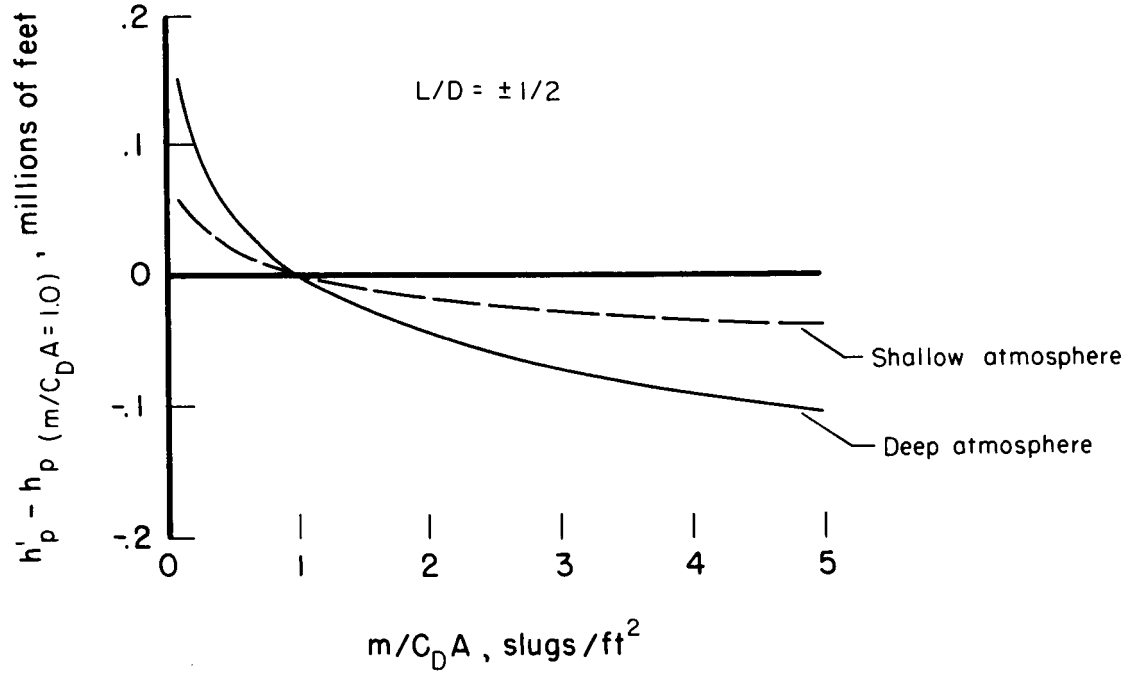

Figure 13.- Effect of $m/C_D A$ on corridor position.

NASA-Langley, 1965 A-984